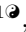
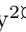


# Gene regulatory networks producing a striped band of gene expression

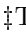
Juan Camilo Arboleda-Rivera<sup>1</sup>, Gloria Machado-Rodríguez<sup>1</sup>, Boris Rodríguez-Rey<sup>2</sup>, Jayson Gutiérrez<sup>3</sup>,


**1** Instituto de Biología, Universidad de Antioquia, Medellín, Antioquia, Colombia


**2** Instituto de Física, Universidad de Antioquia, Medellín, Antioquia, Colombia

**3** Affiliation Dept/Program/Center, Ghent University, Ghent, State, Belgium

 These authors contributed equally to this work.

 These authors also contributed equally to this work.

 Current Address: Dept/Program/Center, Universidad de Antioquia, Medellín, Antioquia, Colombia

 Membership list can be found in the Acknowledgments section.

\* [juan.arboleda2@udea.edu.co](mailto:juan.arboleda2@udea.edu.co)

## Abstract

Lorem ipsum dolor sit amet, consectetur adipiscing elit. Curabitur eget porta erat. Morbi consectetur est vel gravida pretium. Suspendisse ut dui eu ante cursus gravida non sed sem. Nullam sapien tellus, commodo id velit id, eleifend volutpat quam. Phasellus mauris velit, dapibus finibus elementum vel, pulvinar non tellus. Nunc pellentesque pretium diam, quis maximus dolor faucibus id. Nunc convallis sodales ante, ut ullamcorper est egestas vitae. Nam sit amet enim ultrices, ultrices elit pulvinar, volutpat risus.

## Author summary

Lorem ipsum dolor sit amet, consectetur adipiscing elit. Curabitur eget porta erat. Morbi consectetur est vel gravida pretium. Suspendisse ut dui eu ante cursus gravida non sed sem. Nullam sapien tellus, commodo id velit id, eleifend volutpat quam. Phasellus mauris velit, dapibus finibus elementum vel, pulvinar non tellus. Nunc pellentesque pretium diam, quis maximus dolor faucibus id. Nunc convallis sodales ante, ut ullamcorper est egestas vitae. Nam sit amet enim ultrices, ultrices elit pulvinar, volutpat risus.

## Introduction

Cells interact continuously with their environment and they must detect signals from it. In many cases Gene Regulatory Networks (GRNs) interpret these signals through gene interaction and produce a particular response. This information processing function is of particular importance in developmental processes such as those in which a group of cells differentiate in response to a signalling molecule such as a morphogen [1, 2]. However, as information processing by GRNs is often a complex process, one major goal of developmental biology is to understand mechanistically how positional information is translated in spatial differentiation.

Our understanding of how GRNs process information has increased thanks to the concept and theory of network motifs, which are defined as patterns of interconnections occurring in networks at numbers that are significantly higher than those in randomized networks [3]. This novel approach, along with mathematical modeling and computational methods have been shown to be a powerful tool to study GRNs and the predictions of studies using these methods have been validated by experimental studies [4–8].

However, although several studies have analyzed the properties of GRNs that process positional information, they have focused on particular natural networks [9,10], in synthetic networks [8,11,12], or have constrained the design of the GRNs [13].

In this study, we used a set of 2061 three-node GRNs selected by a genetic algorithm to interpret a morphogen signal and respond to it generating a striped pattern of gene expression in order to analyse the role of network motifs in this process and its dynamic properties.

## Materials and methods

### Gene Regulatory Networks and morphogenetic field

In order to study three-node GRNs we represented them by three sets of real numbers, the first set was composed of the interaction values between genes in the network; the second of the diffusion rates ( $D$ ) of each of the three gene products; and the third of the degradation rates ( $\delta$ ) of these same gene products, with  $D$  and  $\delta \in [0, 0.05]$ .

The set of interaction values was represented as adjacency matrices  $W \in \mathbb{R}^{3 \times 4}$  where  $i$  represents a regulated node of the GRN and  $j$  represents a regulator node of the GRN Fig 1 with  $w_{ij} \in [-10, 10]$ . Values in these matrices can be negative, zero or positive and represent repression, no interaction, or activation respectively. The magnitude of the value is proportional to the strength of the interaction.

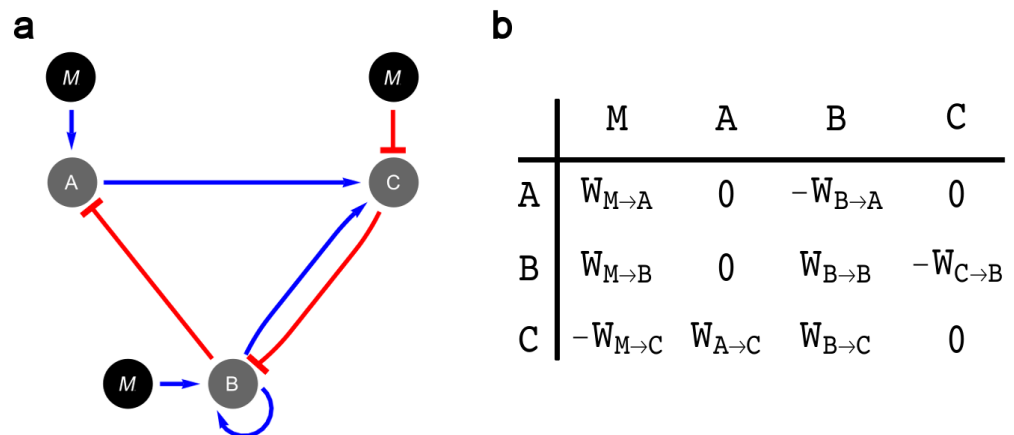


**Fig 1. Modelling of GRNs.**

A: GRN represented as a directed graph with activation (blue arrows) and inhibition (red arrows) interactions. Black circles tagged with a **M** represent the morphogen; **A**, **B** and **C** represent genes in the network. B: The same GRN represented as an adjacency matrix in which positive values represent activation, negative ones represent inhibition and zeros represent no interaction.

In our model the morphogen could interact with any of the three genes on the GRN, but could not be affected by them. The morphogenetic field was defined by an

unidimensional array of 30 isogenic cells exposed to the morphogen concentration gradient (Fig 2). The initial concentration of each gene product in all cells was set to 0.1 in all simulations.

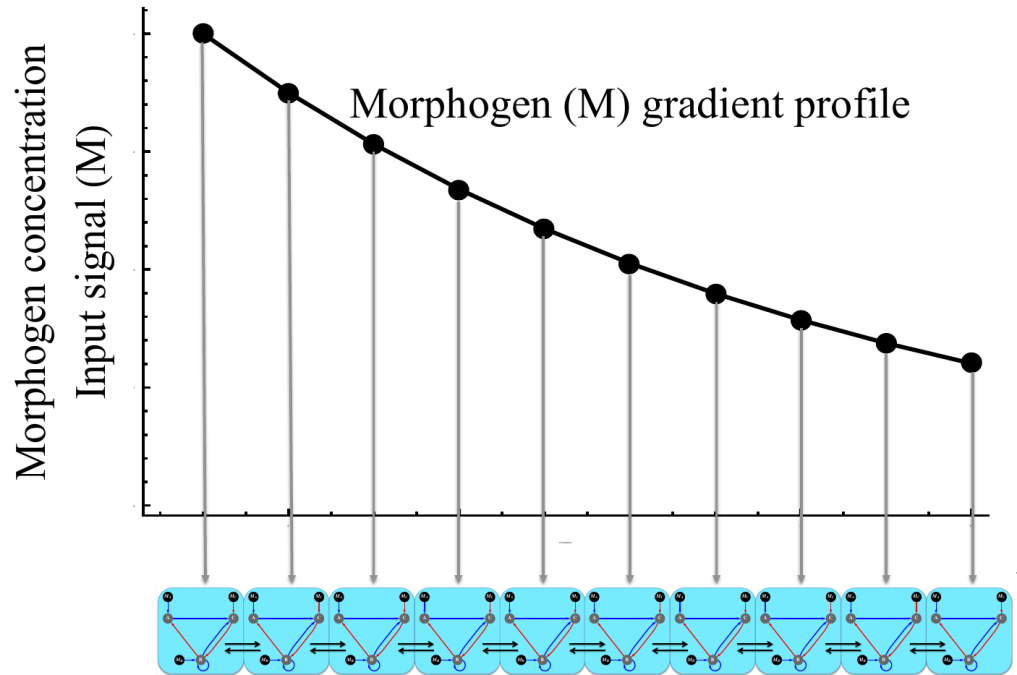


**Fig 2. Morphogenetic field.**

In our model the field was composed of a linear array of 30 isogenic cells and a morphogen gradient concentration described by an exponential decay function. Horizontal arrows between cells represent diffusion of gene products between adjacent cells.

## Mathematical model

Our model is a modification of the model used by Cotterell & Sharpe [14] and proposed by Reinitz et al. [11]. The model is a dynamical system that describes the change in concentration of gene product  $i$  in time, as shown in Eq 1.

$$\frac{d[G]_n^i}{dt} = g(u^i) + D_i \cdot [(G]_{n-1}^i - [G]_n^i) + ([G]_{n+1}^i - [G]_n^i) - \delta_i \cdot [G]_n^i, \quad (1)$$

in which  $[G]_n^i$  is the concentration of the  $i$ -th gene in the  $n$ -th cell ( $[G]_n^i \geq 0$ ),  $g(u^i)$  is a function describing the relationship between the interactions on the  $i$ -th gene and its expression Eq (2) and described in more detail below.  $D_i$  and  $\delta_i$  are the diffusion and the degradation rate of  $i$ -th gene product, respectively.

The input function is a sigmoid function described by Eq 2.

$$g(u^i) = \frac{1}{1 + \exp(a - b \cdot u^i)}, \quad (2)$$

in which  $a$  is the sigmoid steepness, equal to 5;  $a/b$  is the threshold value, set to 1 for all simulations, and  $u^i$  is the following equation:

$$u^i = \sum_j w_{ij} \cdot [G]_n^j + w_{im} \cdot [M]_n. \quad (3)$$

This equation sums the interactions acting upon the  $i$ -th gene, being  $w_{ij}$  the interaction strength of the  $j$ -th gene upon the  $i$ -th gene and  $w_{im}$  the interaction strength of the morphogen upon the  $i$ -th gene.  $[G]_n^j$  and  $[M]_n$  are the concentrations of the  $j$ -th gene product and the morphogen in the  $n$ -th cell.

## Morphogen spatial distribution

The morphogen concentration along the morphogenetic field is described by Eq 4.

$$M = A_0 \cdot \exp(-c/h), \quad (4)$$

where  $A_0$  is the concentration of the morphogen in the position zero of the morphogenetic field and was set to 1 in our experiments;  $c$  is the cell index, defined as the ratio between the  $n$ -th cell from left to right and the total number of cells, and  $h$  is a decay parameter, whose value in our model was set to 0.4.

The phenotype of a GRN was defined as the expression pattern of each gene along the morphogenetic field after 500 time steps of integration of the dynamical system. We chose that number of time steps because numerical experiments showed that GRNs reached the steady state in approximately 300 steps.

## Optimal pattern definition

The optimal pattern of gene expression defined by us, consisted in cells at the sides of the field ( $n < 11$  and  $n > 20$ ) displaying expression levels lower than 10% of the maximal level observed along the field of cells for the output gene, and cells at the middle of the field ( $n \in [11, 20]$ ) displaying expression levels greater than 90% of the maximal level observed along the entire field for the output gene (Fig 3).

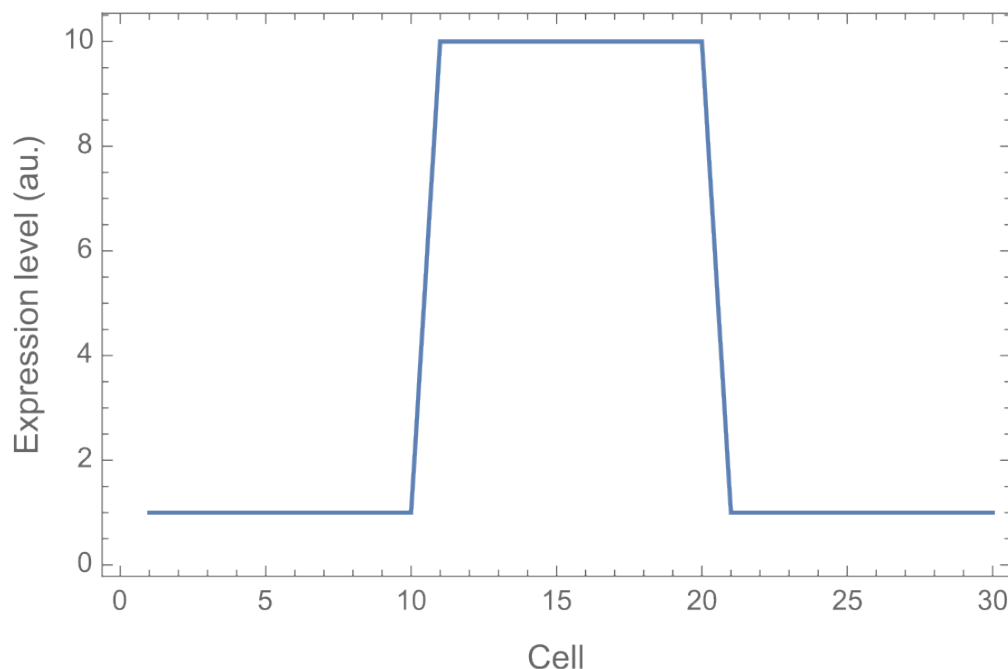


**Fig 3. Optimal gene expression pattern.**

## Genetic algorithm

The genetic algorithm used to produce the set of gene regulatory networks (GRNs) consisted in the following steps:

1. **Generate a set of 200 random GRNs.**
2. **Numerically solve the dynamical system for each GRN from  $t=0$  until  $t=500$ .** We integrated the differential equation using the function NDSolve from Wolfram Mathematica 11 with the option “EquationSimplification” and the “Residual” simplification method.
3. **Evaluate fitness by comparing the phenotypes with the optimal phenotype (Fig 3).** In order to compute the fitness function for each GRN we used three different filters. The first filter assesses whether the expression profile of the output node reaches a quasi-steady state:

$$S_{filter} = \left( \frac{1}{I \cdot N} \right) \sqrt{\sum_{i=1}^{I=3} \sum_{n=1}^{N=30} ([G]_n^i(t=500) - [G]_n^i(t=250))^2}. \quad (5)$$

The expression profile was considered to have reached the steady state if  $S_{filter} < 0.001$ .

The second filter measures the spatial heterogeneity in the field:

$$P_{filter} = \left( \frac{1}{I \cdot N} \right) \sqrt{\sum_{i=3}^{I=3} \sum_{n=1}^{N=30} ([G]_n^i - \langle [G]_n^i \rangle)^2}, \quad (6)$$

where  $\langle [G]_n^i \rangle$  is the mean concentration of the  $i$ -th gene along the field at  $t = 500$ . The third filter relates the Manhattan Distance ( $D_{obs}$ ) between an expression pattern and the optimal pattern with the maximum distance achievable ( $D_{max}$ ):

$$PF_{eff} = 1 - \frac{D_{obs}}{D_{max}}. \quad (7)$$

In this function, the expression profile of the output gene was normalized and discretized so that each expression value for each cell in the field was an integer ranging from 1 to 10.

The filters mentioned above are integrated in the following functions that assess the quality of a given phenotype:

$$Q_1(P_{filter}) = \left( \frac{P_{filter}^{10}}{P_{filter}^{10} + 0.1^{10}} \right), \quad (8)$$

$$Q_2(S_{filter}) = \left( \frac{0.1^2}{S_{filter}^2 + 0.1^2} \right). \quad (9)$$

Finally, these quality functions were used to compute the fitness score with the following fitness function:

$$F = PF_{eff} \cdot Q_1(P_{filter}) \cdot Q_2(S_{filter}). \quad (10)$$

4. **Select GRNs with a probability proportional to its fitness.**

5. **Recombine and mutate GRNs.** Mutations included changes in the numerical values of degradation and diffusion parameters and interaction strengths, and addition and removal of interactions among genes and between the genes and the morphogen.

Steps 2 to 5 were iterated 1000 times, resulting in a set of 2061 GRNs with a striped pattern of gene expression in at least one gene.

## Classification of GRNs

In order to group all the isomorphic networks in the set of 2061 GRNs we used a classification algorithm that selected a random GRN, then it generated all isomorphs of that GRN by performing permutations in rows and columns. The algorithm then compared all six isomorphs with other GRN and classified the topologies in the same group if they were isomorphic networks.

## Neutral network

The neutral network was obtained by generating all possible isomorphs of a network topology and then calculating the minimal Hamming distance between these isomorphs and other network topologies. The Hamming distance between two topologies was calculated using the following equation:

$$D_H(W^A, W^B) = \sum_{ij} | \text{sgn}(w_{ij}^A) - \text{sgn}(w_{ij}^B) | . \quad (11)$$

We adopted the same definition of neighborhood as Cotterell & Sharpe [14], in which two topologies were neighbors if the gain or removal of any one interaction can transform one of the topologies into the other.

## Robustness analysis

In order to evaluate the robustness of the different topologies to perturbations in parameters of interactions between genes we took a GRN belonging to each one of the network topologies and we modified each interaction independently by increasing and decreasing its value in a 20%. For topologies with 3 or more GRNs we chose the most similar to the mean configuration for that topology.

As a measure of the robustness of the topology we chose the proportion of times in which a perturbation resulted in a GRN with a fitness greater or equal to 0.95. Additionally, we considered a topology to be robust if the previous measure was greater or equal to 0.5.

As a measure of the robustness of subgraphs (see “Classification of topologies”) we calculated the mean of the robustness measure of all the topologies containing a particular subgraph.

## Robustness of topology 9 to perturbations in non-network parameters

In order to estimate the robustness of topology 9 to changes in parameters that control morphogen gradient and changes in initial concentrations of gene products, we generated 100 fitness values for each one of the 19 GRNs belonging to topology 9; in each of these 100 assays we chose  $A_0$ ,  $h$  or initial concentrations randomly from a Normal Distribution with  $\mu = 1$  for  $A_0$ ,  $\mu = 0.4$  for  $h$  and  $\mu = 1$  for initial concentrations and a Coefficient of Variation of 30% in each case.

## Shannon entropy

We calculated the Shannon entropy Eq (12) of the network topologies distribution in order to test if this distribution could be obtained by chance with a probability greater than 0.05. In order to obtain a 95% confidence interval, we generated 30 samples of a set of 2061 random matrices and calculated the Shannon entropy in bits for each sample and tested these data for normality.

$$H = - \sum p(x) \cdot \log_2 p(x). \quad (12)$$

## Classification of GRNs phenotypes

In order to classify each GRN by its spatiotemporal expression profile (its dynamics of expression), we selected expression profiles of GRNs from time step 0 to time step 250 each 10 time steps, for a total of 26 expression profiles over time. These spatiotemporal expression profiles were represented as tensors  $S \in \mathbb{R}^{3 \times 26 \times 30}$ , in which each element ( $s_{itn} \geq 0$ ) is the expression level of the  $i$ -th gene at time  $t$  in cell  $n$ .

Later we calculated the distance between all the pairs of tensors and we performed a Neighbor Joining clustering using the package Scikit Bio 0.5.5 from Python 3.

## Classification of topologies

In order to classify each topology by its subgraph composition, we first created a matrix  $T = (t_{ij})$  with 714 rows corresponding to each different topology and 17 columns corresponding to different subgraphs. Each element  $t_{ij}$  of the matrix was 1 if the  $j$ -th subgraph was present in the  $i$ -th topology or 0 if the subgraph was not present.

With this matrix we then calculated a distance matrix in which each element consisted in the Hamming distance between the row vectors in matrix  $T$  between each pair of topologies. We then performed a clustering of these topologies using the Neighbor Joining method in the Scikit Bio package.

## Complexity index and network descriptors

As a measure of network complexity, we used the complexity index based on Shannon entropy proposed by Bonchev & Rovray [15]. We calculated this index using the following equation:

$$I_{vd} = \sum_{i=1}^V a_i \cdot \log_2 a_i, \quad (13)$$

being  $a_i$  the degree of  $i$ -th node and  $V$  the number of nodes in the network. The network descriptors were calculated using built-in functions from Wolfram Mathematica software.

We performed a Pearson's chi-square goodness of fit test for the node degree distribution using Wolfram Mathematica.

## Results

The classification of GRNs showed that in our initial set of 2061 GRNs exists a number of 714 different network topologies, each one of them containing a different number of GRNs (Fig 4). This abundances distribution was not produced by chance (Shannon entropy = 8.52963, 95% confidence interval = [10.8915, 10.9275]), and instead it shows a structuring, indicating the possible existence of network motifs.

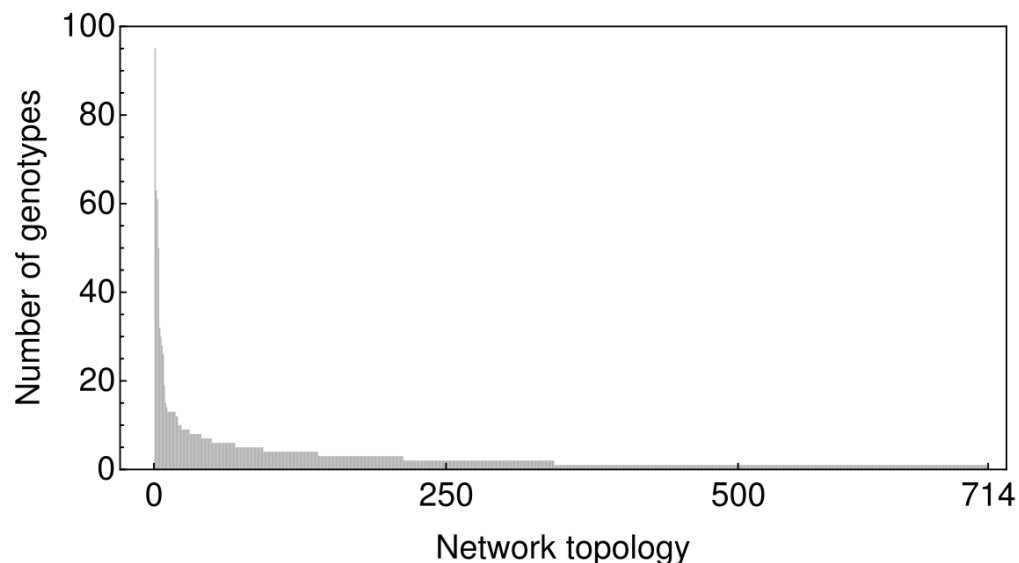


**Fig 4. Distribution of abundances of network topologies.**

The most abundant network topologies are shown in Fig 5. Interestingly, among the 15 most abundant network topologies, eleven of them presented the Incoherent type 3 Feed-Forward Loop (I3-FFL) network motif. In addition, we found that topology number 9 could produce the striped phenotype with only two nodes.

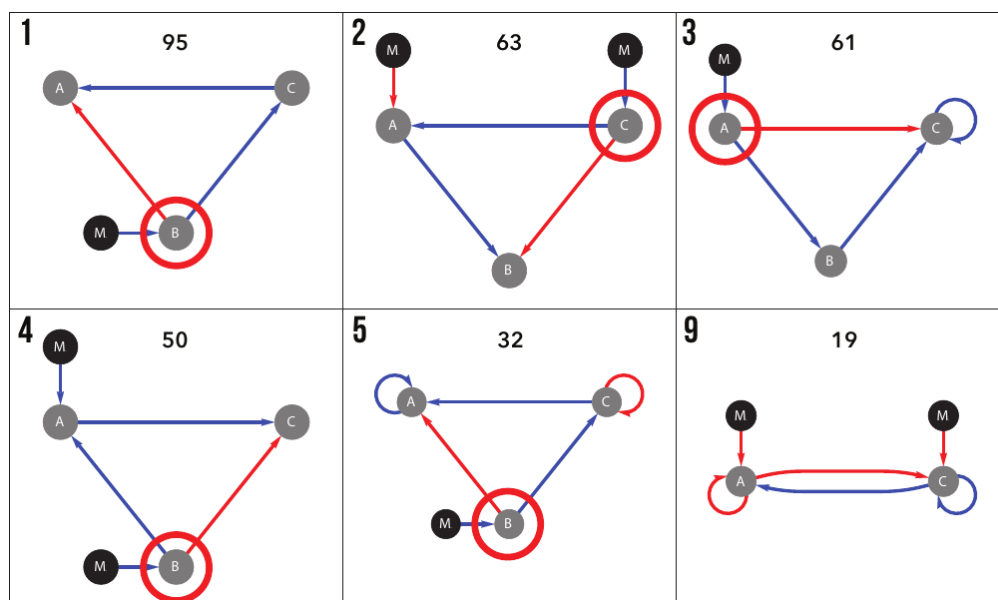


**Fig 5. Most frequent network topologies.**

In this figure we show the most frequent network topologies, which contain the I3-FFL network motif. Top left of each box is presented the network topology number in order of abundance. Top center is presented the number of GRNs belonging to that network topology. Circled in red are the input nodes of I3-FFL in network topologies 1 to 5, that display the striped pattern of gene expression using three nodes, in contrast, network topology number 9 displays the same phenotype using a two-node GRN.



The neutral network shows that most of the network topologies are grouped into a connected graph. This graph is composed of 639 nodes that are accessible by one mutational step. The 15 most abundant network topologies, with the exception of number 10, are located in this graph (Fig 6). We also found nodes inside the neutral network that had more connections between them than with other nodes, generating thus clusters of nodes, interestingly in almost every cluster is present one or more of the most abundant network topologies. In addition, we found that the first eight most abundant network topologies were located in the largest cluster.

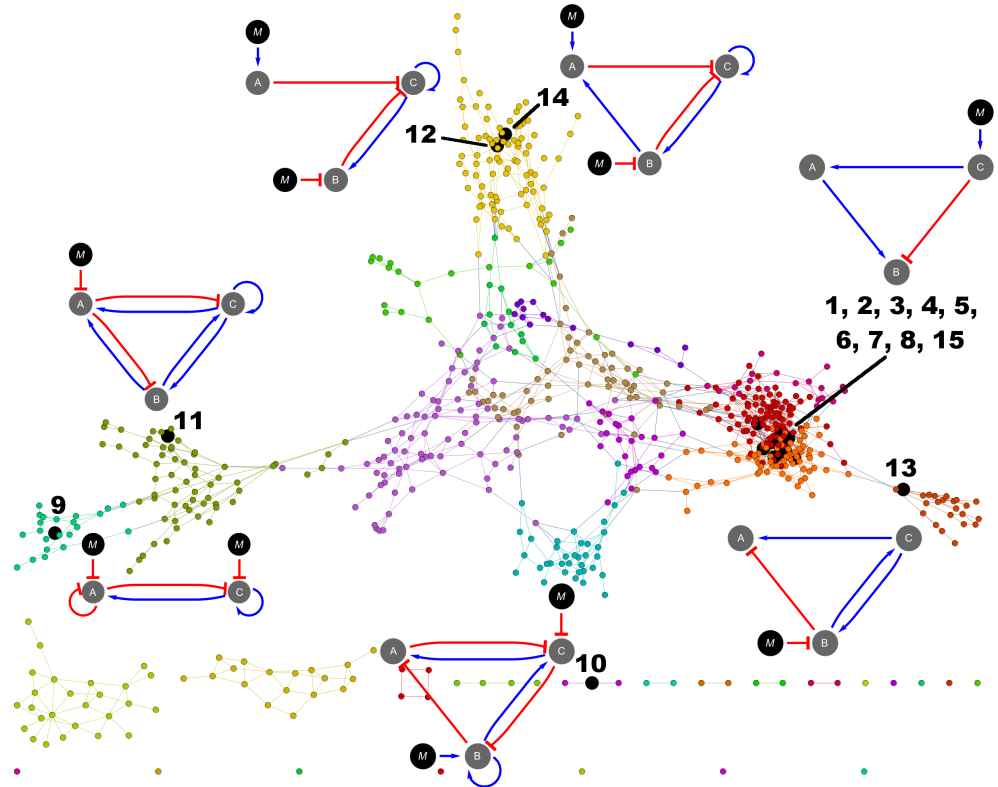


**Fig 6. Neutral network.**

This graph shows network topologies connected by one mutational step. Most abundant network topologies are shown as black nodes. All nodes with the same color belong to a cluster of nodes more connected between them than with other nodes in the graph.

The degree distribution of this network seems to follow a Poisson distribution (Pearson's  $\chi^2 = 12.8902$ , p-value = 0.115684) characteristic of a Erdős-Rényi network [16]. This kind of network presents a great number of nodes with low degree and a few nodes with high degree (Fig 7). Nodes corresponding to topologies number one and three showed the highest degree ( $deg(1) = deg(3) = 14$ ). Curiously, nodes with higher degree resulted to be also those network topologies with higher abundance (Fig 8), indicating a high robustness to topological mutations as well as robustness to mutations in the parameter values. This relationship between abundance and node degree was corroborated by the Spearman correlation ( $r_s = -0.353752$ ,  $p = 6.2933 \times 10^{-23}$ ).

We wanted to know if connecting topologies separated by two mutational steps would produce a connected graph, for that reason we generated another neutral network joining neighbors at two mutational steps and we found that only topology number 420 remained unconnected from the rest of topologies in the graph (Fig 9).

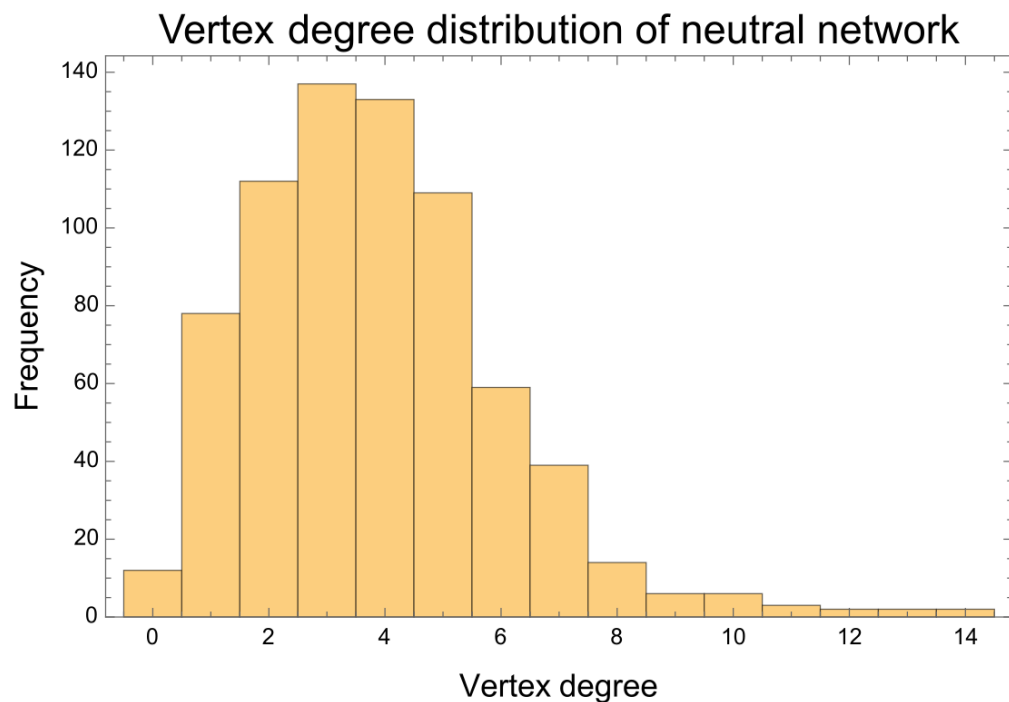


Fig 7. Histogram of vertex degree distribution in the neutral network.

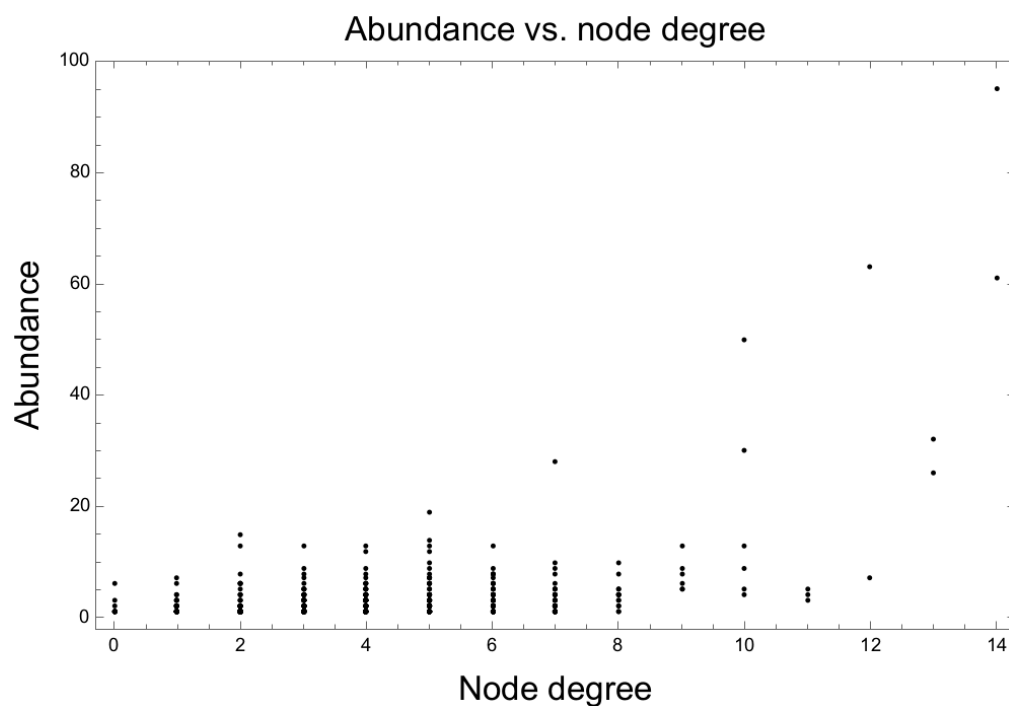
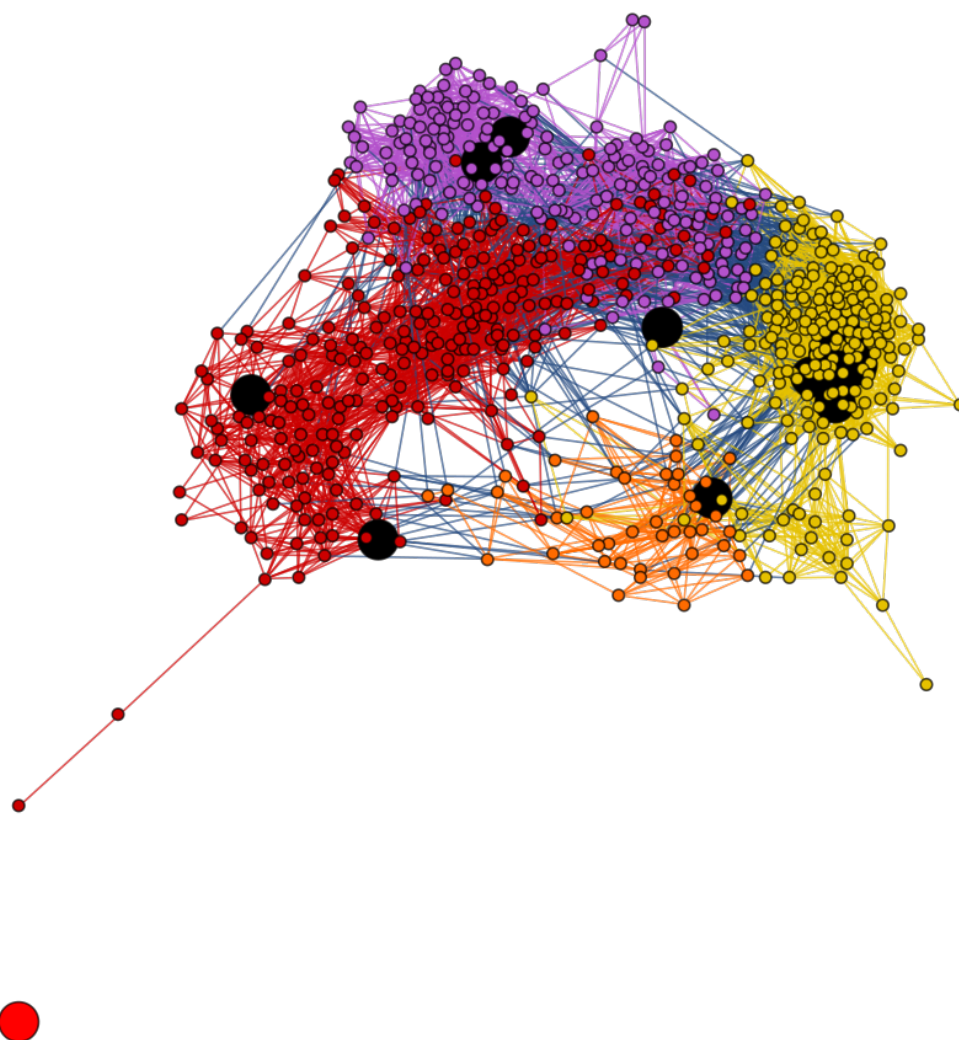


Fig 8. Scatter plot of Topology abundance vs. Node degree in the neutral network.

Besides topological robustness, we wanted to know if network topologies were robust to perturbations in the values of the parameters. After performing the perturbations to a GRN from each topology, we plotted the abundance of the topology vs. its robustness.



**Fig 9. Network of topologies separated by two mutational steps.**

The network shows that all the topologies are connected by two or less mutational steps, except for topology number 420 (big red circle). Big black circles correspond to the 15 topologies with higher abundance.

We did not find a significant correlation between these two variables ( $r_S = -0.0389724$ , p-value = 0.298475) (Fig 10). However, when we grouped those topologies containing the same subgraph and calculated their mean robustness, we found that between the most robust subgraphs is the “Bistable” motif reported by Cotterell & Sharpe [14], the I3-FFL and the “Overlapping domains” motif (which is a variation of the I3-FFL) also reported by Cotterell & Sharpe (see Supplementary Material).

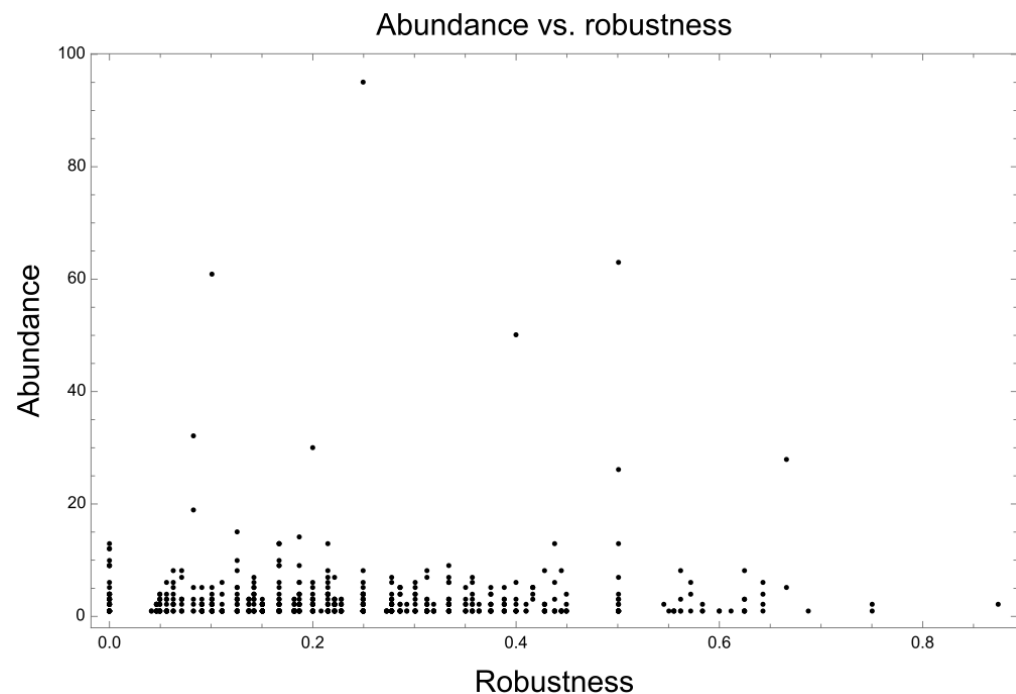


**Fig 10. Scatter plot of Abundance vs. robustness.**

The robustness of each topology was calculated as the number of perturbations in which the fitness was greater or equal to 0.95 with respect to the total of perturbations performed.

The average vertex degree indicates that in general all the network topologies display high robustness and that they could resist an average of approximately 4 topological mutations without losing their fitness. Additionally, the average path length indicates that the evolutionary landscape is easily accessible for most network topologies (Table 1).

**Table 1. Network descriptors of neutral network of topologies.**

Network descriptor	Value
Average vertex degree	3.85714
Clustering coefficient [17]	0.117097
Average path length	7.25261
Graph connectedness	0.00540974
Graph diameter*	25
Average path length*	9.0499

\*These descriptors were calculated for the main connected subgraph of the network.

The average complexity index of network topologies was 39.2435 ( $\pm 11.6768$ ) and was found to be negatively correlated with the abundance ( $r_S = -0.316653$ ,

p-value =  $2.25161 \times 10^{-18}$  (Fig 11).

217

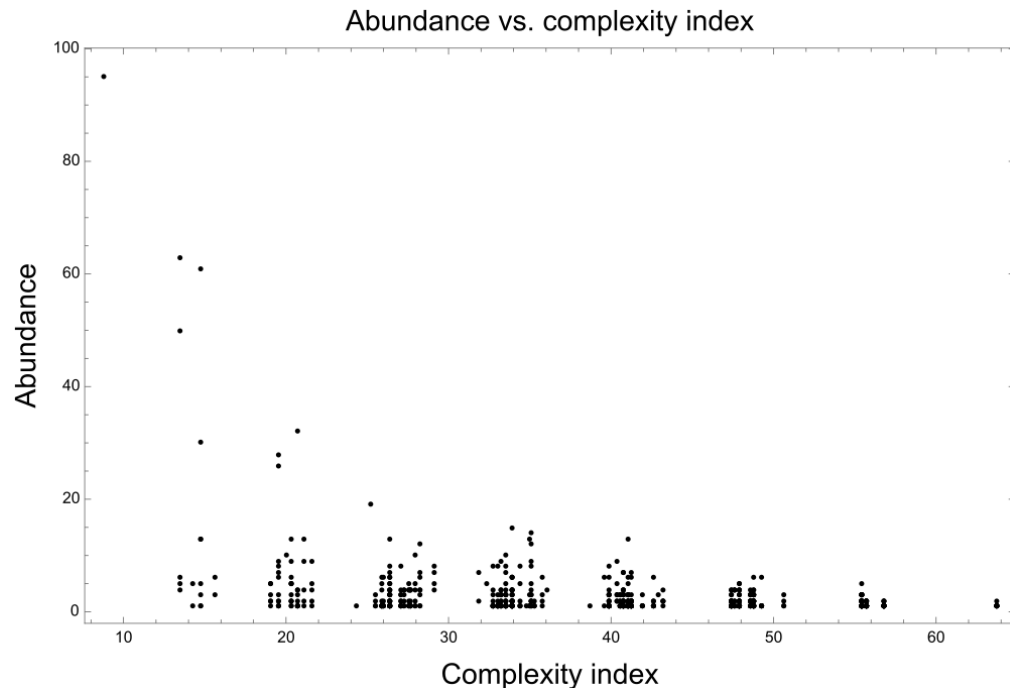


**Fig 11. Scatter plot of Abundance vs. Complexity index.**  
Each point in the plot represents one of the 714 network topologies.

Spatiotemporal expression profiles showed that all GRNs reached a steady state expression profile before  $t = 250$  and most of them indeed reached the steady state before  $t = 150$  (Fig 12).

218

219

220

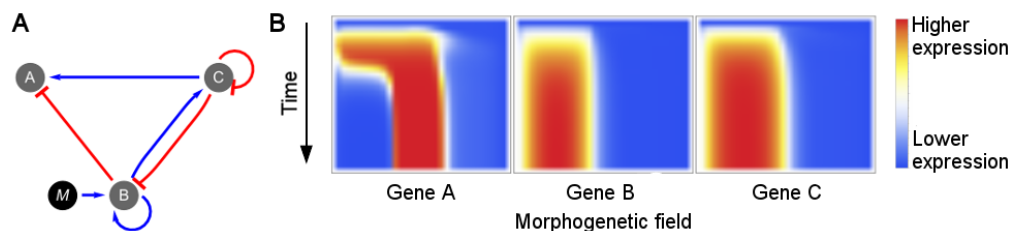


**Fig 12. Most GRNs reach the steady state before 250 time steps.**  
GRN number 660 displaying the topology number 33 (A) and its spatiotemporal expression profile (B).

Hierarchical clustering of spatiotemporal expression profiles showed that GRNs with topologies that seemed to be very different have indeed very similar expression dynamics. We expected to find GRNs with the same topology to group together but instead we found GRNs with different topologies grouped as sister taxa (Fig 13). More interestingly, some GRNs displaying very abundant network topologies are grouped together with GRNs displaying very infrequent network topologies.

221

222

223

224

225

226

Clustering of topologies revealed that there are six main groups of topologies in our set of 2061 GRNs (Fig 14).

227

228

Among the new network topologies we report here, perhaps the most interesting is the topology number 9, which is able to express the striped gene expression pattern with only two genes and indeed expresses this pattern in both genes (Fig 15).

229

230

231

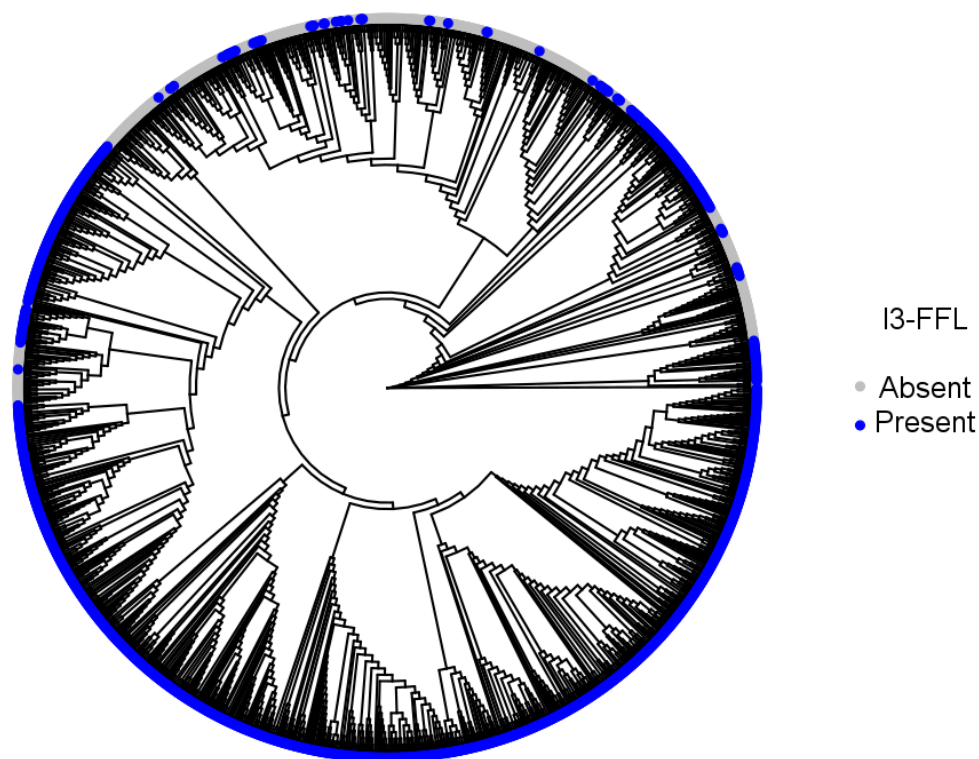


**Fig 13. Clustering of spatiotemporal expression profiles obtained by neighbor joining showing the presence of I3-FFL network motif.**

Although the topology 9 consists of only two genes, its mechanism of expression is dynamically more complex than that of other topologies such as the simple I3-FFL. Initially the expression pattern of the gene A is uniform in the morphogenetic field, but later it is shaped by the morphogen gradient in such a way that two important events occur, in first place the overall expression level of the gene A is decreased by the inhibition of the morphogen, releasing gene C from its repression by gene A; in second place, appears a non-homogeneous spatial distribution in which gene A is expressed at higher levels in the cells at the rightmost part of the morphogenetic field.

These two events conduce to the repression of the gene C by the gene A in the rightmost part of the morphogenetic field and by the morphogen in the leftmost part of the morphogenetic field, thus generating a lightly higher level of expression of gene C in the center of the field. Because gene C activates its own expression, a band of expression begins to form. This band of expression then begins to activate the gene A also in the center of the field (Fig 16).

In this way two bands of expression are formed that depend on each other. The high level of gene C in the middle of the field counteract its inhibition by gene A, while in the ends of the bands the inhibition of gene A on gene C overcomes the self-activation of gene C, preventing the expression of the latter to extend out of the middle of the field. In turn, the band of expression of gene A can only exist in the middle of the field because its expression depends on gene C.

This is a complex mechanism described by the first time in this study, and it would be interesting to study its feasibility and possible implementation in synthetic gene regulatory networks.

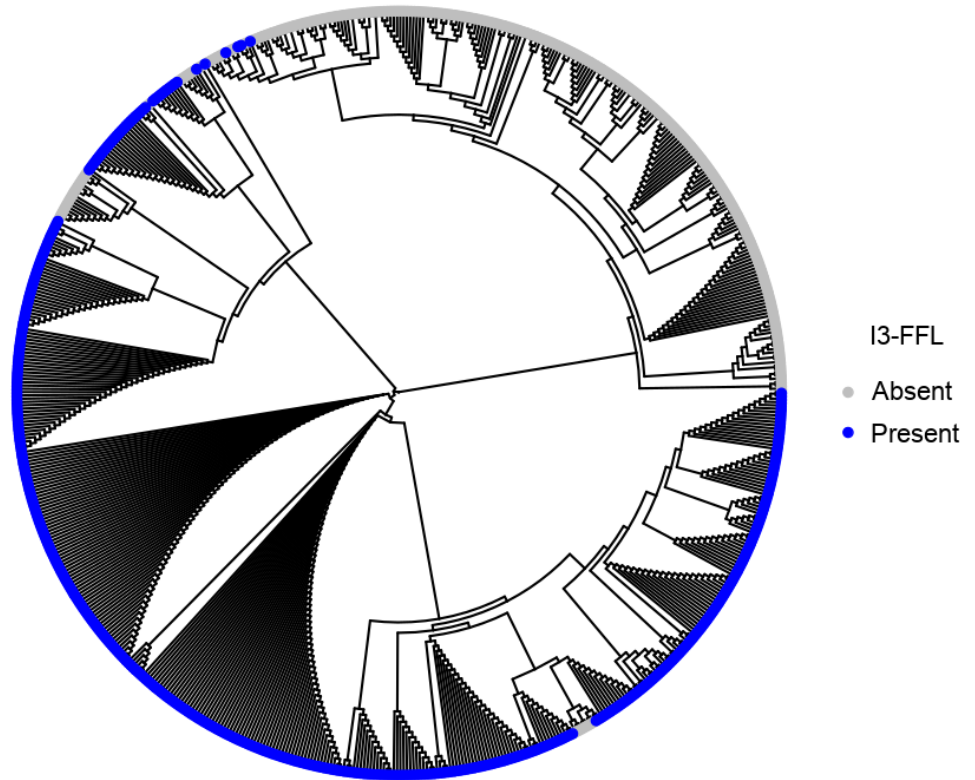


**Fig 14. Clustering of network topologies.**  
Blue circles correspond to topologies that contain the I3-FFL network motif.

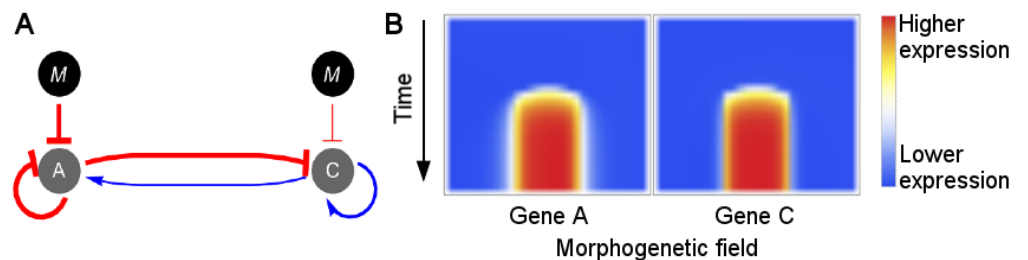


**Fig 15. Expression dynamics of topology 9.**  
A: Network topology number 9. B: Spatiotemporal expression profile of a GRN with topology 9.

## Discussion

We found the presence of network motifs in the GRNs produced by the genetic algorithm. However, we also found a great diversity of network topologies that could produce a striped gene expression pattern.

We found that the I3-FFL is one of the network motifs that appears more frequently in these GRNs, as has also been reported by Cotterell & Sharpe [14], and has been found in transcriptional networks involved in cell fate definition [18]. Moreover, our results indicate that this is a robust motif that can be useful for construction of synthetic gene regulatory networks that are exposed to stochastic fluctuations in the environment and mutations.



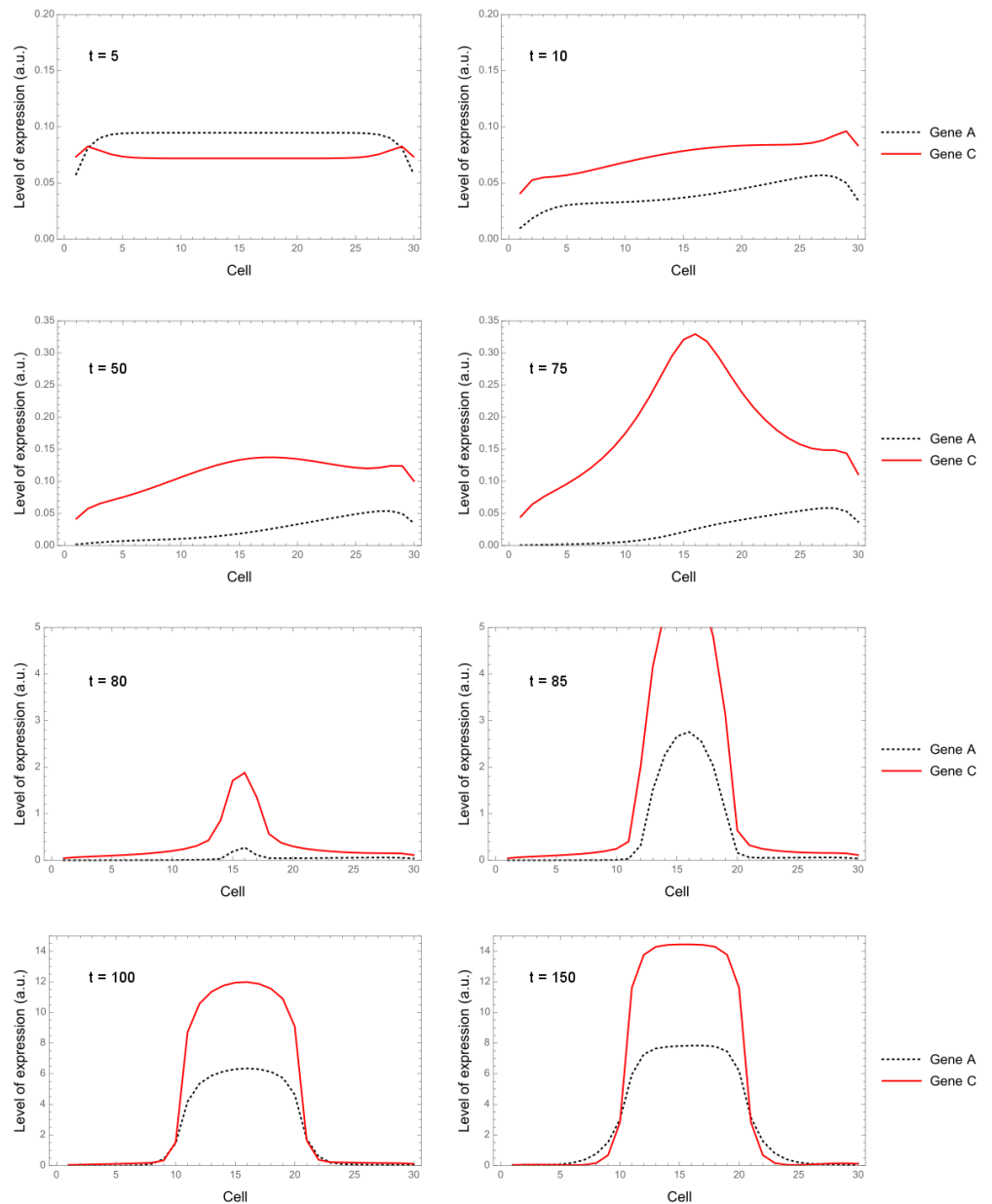


**Fig 16. Dynamics of expression in topology number 9.**

However, as our model was less stringent, we found a larger number of possible topologies with the same striped phenotype.

Although it has been experimentally demonstrated that the Incoherent Feed Forward Loop type 2 (I2-FFL) is able to generate a striped gene expression pattern, [8,9], in our study this motif was present in only 10.92% of the topologies. This fact may be because genetic algorithms can not always find global minima but local minima or its surroundings, however, it is also possible that the I2-FFL motif is not as robust as other motifs and therefore be less represented.

We also found topologies with a similar topology to that of the “opposing gradients” reported by Schaerli et al. [9,12]. Although the “opposing gradients” mechanism requires the constitutive expression of two of the genes in the GRN, and our model does



not take constitutive expression into account, we realized that the GRNs that presented the “opposing gradients” topology, had also commonly positive auto-regulation interactions on these two nodes, supplying in this way the lack of constitutive expression.

The correlation between the complexity index of a topology and its abundance indicates that networks with simpler designs are more robust to changes in interaction parameters and that more complex networks are less robust. For example, topology number 420, which presents high complexity, was one of the topologies with lower abundance and was disconnected from all other topologies in the two-step neighbors in the neutral network.

It is interesting that the one-step neutral network

## Conclusion

This study can help us to understand the mechanisms by which the GRNs work in nature as modules that make part of genomes, but it also can provide guidance in the construction of new synthetic GRNs in the field of synthetic biology.

## Supporting information

**S1 Fig. Bold the title sentence.** Add descriptive text after the title of the item (optional).

**S2 Fig. Lorem ipsum.** Maecenas convallis mauris sit amet sem ultrices gravida. Etiam eget sapien nibh. Sed ac ipsum eget enim egestas ullamcorper nec euismod ligula. Curabitur fringilla pulvinar lectus consectetur pellentesque.

**S1 File. Lorem ipsum.** Maecenas convallis mauris sit amet sem ultrices gravida. Etiam eget sapien nibh. Sed ac ipsum eget enim egestas ullamcorper nec euismod ligula. Curabitur fringilla pulvinar lectus consectetur pellentesque.

**S1 Video. Lorem ipsum.** Maecenas convallis mauris sit amet sem ultrices gravida. Etiam eget sapien nibh. Sed ac ipsum eget enim egestas ullamcorper nec euismod ligula. Curabitur fringilla pulvinar lectus consectetur pellentesque.

**S1 Appendix. Lorem ipsum.** Maecenas convallis mauris sit amet sem ultrices gravida. Etiam eget sapien nibh. Sed ac ipsum eget enim egestas ullamcorper nec euismod ligula. Curabitur fringilla pulvinar lectus consectetur pellentesque.

**S1 Table. Lorem ipsum.** Maecenas convallis mauris sit amet sem ultrices gravida. Etiam eget sapien nibh. Sed ac ipsum eget enim egestas ullamcorper nec euismod ligula. Curabitur fringilla pulvinar lectus consectetur pellentesque.

## Acknowledgments

Cras egestas velit mauris, eu mollis turpis pellentesque sit amet. Interdum et malesuada fames ac ante ipsum primis in faucibus. Nam id pretium nisi. Sed ac quam id nisi malesuada congue. Sed interdum aliquet augue, at pellentesque quam rhoncus vitae.

## References

1. Turing AM. The chemical basis of morphogenesis. *Bulletin of Mathematical Biology*. 1952;52(1-2):153–197. doi:10.1007/BF02459572.
2. Wolpert L. Positional information and the spatial pattern of cellular differentiation. *Journal of Theoretical Biology*. 1969;25(1):1–47. doi:https://doi.org/10.1016/S0022-5193(69)80016-0.
3. Milo R, Shen-Orr SS, Itzkovitz S, Kashtan N, Chklovskii D, Alon U. Network Motifs: Simple Building Blocks of Complex Networks. *Science*. 2002;298(5594):824–827. doi:10.1126/science.298.5594.824.
4. Kalir S, Mangan S, Alon U. A coherent feed-forward loop with a SUM input function prolongs flagella expression in *Escherichia coli*; 2005.
5. Kalir S, Alon U. Using a quantitative blueprint to reprogram the dynamics of the flagella gene network. *Cell*. 2004;117(6):713–720. doi:10.1016/j.cell.2004.05.010.
6. Mangan S, Zaslaver A, Alon U. The coherent feedforward loop serves as a sign-sensitive delay element in transcription networks. *Journal of molecular biology*. 2003;334(2):197–204.
7. O'Donnell KA, Wentzel EA, Zeller KI, Dang CV, Mendell JT. c-Myc-regulated microRNAs modulate E2F1 expression. *Nature*. 2005;435(7043):839–843. doi:10.1038/nature03677.
8. Basu S, Gerchman Y, Collins CH, Arnold FH, Weiss R. A synthetic multicellular system for programmed pattern formation. *Nature*. 2005;434(7037):1130–1134. doi:10.1038/nature03461.
9. Schaerli Y, Munteanu A, Gili M, Cotterell J, Sharpe J, Isalan M. A unified design space of synthetic stripe-forming networks. *Nature Communications*. 2014;5(May):4905. doi:10.1038/ncomms5905.
10. Jaeger J, Blagov M, Kosman D, Kozlov KN, Manu, Myasnikova E, et al. Dynamical analysis of regulatory interactions in the gap gene system of *Drosophila melanogaster*. *Genetics*. 2004;167(4):1721–1737. doi:10.1534/genetics.104.027334.
11. Reinitz J, Mjolsness E, Sharp DH. Model for cooperative control of positional information in *Drosophila* by bicoid and maternal hunchback. *Journal of Experimental Zoology*. 1995;271(1):47–56. doi:10.1002/jez.1402710106.
12. Schaerli Y, Jiménez A, Duarte JM, Mihajlovic L, Renggli J, Isalan M, et al. Synthetic circuits reveal how mechanisms of gene regulatory networks constrain evolution. *Molecular Systems Biology*. 2018;14(9):e8102. doi:10.15252/msb.20178102.
13. Elowitz MB, Leibier S. A synthetic oscillatory network of transcriptional regulators. *Nature*. 2000;403(6767):335–338. doi:10.1038/35002125.
14. Cotterell J, Sharpe J. An atlas of gene regulatory networks reveals multiple three-gene mechanisms for interpreting morphogen gradients. *Molecular Systems Biology*. 2010;6(425):1–14. doi:10.1038/msb.2010.74.
15. Bonchev DG, Rouvray DH. Complexity in Chemistry, Biology, and Ecology, ser. Mathematical and Computational Chemistry. Springer; 2005.

16. Erdős P, Rényi a. On random graphs. *Publicationes Mathematicae*. 1959;6:290–297. doi:10.2307/1999405.
17. Watts DJ, Strogatz SH. Collective dynamics of 'small-world' networks. *Nature*. 1998;393(6684):440–2. doi:10.1038/30918.
18. Li L, Rispoli R, Patient R, Ciau-Uitz A, Porcher C. Etv6 activates vegfa expression through positive and negative transcriptional regulatory networks in *Xenopus* embryos. *Nature Communications*. 2019;10(1). doi:10.1038/s41467-019-09050-y.